

ANALYTIC ANALYSIS OF THE FEATURES OF GaAs/Si RADIAL HETEROJUNCTIONS: INFLUENCE OF TEMPERATURE AND CONCENTRATION

Jo'shqin Sh. Abdullayev^{a,*}, Ibrokhim B. Sapaev^{a,b}

^aNational Research University TIIAME, Department of Physics and Chemistry, Tashkent, Uzbekistan

^bWestern Caspian University, Baku, Azerbaijan

*Corresponding Author e-mail: j.sh.abdullayev6@gmail.com

Received November 7, 2024; revised January 6, 2025; accepted January 8, 2025

In this article, we analytically study the electrophysical features of the p-Si/n-GaAs radial heterojunction (RHJ) over a temperature range of 50 K to 500 K, in increments of 50 K while considering various doping concentrations. The analysis encompasses band gap narrowing (BGN), the differences in the band gap between GaAs and Si as a function of temperature, and the built-in potential relative to temperature. In particular, we focus on core p-Si with a radius of 0.5 μm and shell n-GaAs with a radius of 1 μm within the structure. Our findings indicate that the thickness of the depletion region in the p-Si/n-GaAs (RHJ) increases with rising temperature. The band gap difference between GaAs and Si is 0.31 eV at 300 K in our model, which is in good agreement with the experimental results. Additionally, the conduction band offset $\Delta E_c=0.04$ eV and the valence band offset $\Delta E_v=0.27$ eV were calculated at 300 K. When the doping concentration changes from $2 \cdot 10^{15}$ to $2 \cdot 10^{18}$ band gap narrowing (BGN) decreases by 2 meV. Additionally, the built-in potential of the p-Si/n-GaAs (RHJ) decreases by 76 mV with increasing temperature.

Keywords: Radial p-n junction; Light trap; External factors; Volt-farad; Heterostructures; Radial heterojunction (RHJ); Band gap narrowing (BGN); Cryogenic temperatures

PACS: 73.40. Lq, 73.61.Cw, 73.61.Ey, 72.20.Jv

INTRODUCTION

The rapid progress in semiconductor electronics research has led to substantial advancements in the design, optimization, and functionality of modern devices. Key innovations, such as two-dimensional transistors [1], nanowires [2], and notably, radial p-n junction structures [3,4], have expanded the potential for nanoscale applications. Among these, radial p-n junctions offer distinct advantages over conventional planar configurations, particularly in submicron nanowires [5,6]. Over the past two decades, these structures have gained prominence due to their superior optical and electronic characteristics, making them highly suitable for applications in photodiodes, optical sensors [7], thermal detectors, photovoltaic detectors [8], and solar cells [9]. By optimizing light absorption and carrier collection, radial p-n junctions reduce optical losses, thereby enhancing energy conversion efficiency. Their perpendicular orientation for light absorption and carrier transport further supports high-frequency applications, including high-speed electronics and wireless communication. Radial junctions also play a critical role in high-speed photodetectors [10], avalanche photodiodes [11], photovoltaic devices, gamma-ray detectors [12], and infrared sensors [13,14], where their structure provides outstanding efficiency, speed, and sensitivity essential for advanced semiconductor applications. Given the broad application range of these junctions, a detailed investigation of their electrophysical properties particularly ionization processes and performance across diverse temperatures is crucial. Both theoretical modeling and experimental validation are necessary to achieve the high reliability and accuracy required for these devices. While radial p-n and p-i-n junctions have been widely explored, heterojunction structures are less extensively studied. Despite the development of new semiconductor materials, GaAs remain the primary material for optoelectronic devices, while Si continues to be the most widely used material due to its advanced technological development and abundance on the Earth's surface. From this perspective, the p-Si/n-GaAs (RHJ) has been selected for this study. This work addresses this gap by focusing on the p-Si/n-GaAs (RHJ) structure, analyzing its electrophysical properties through theoretical and analytical methods. We apply mathematical modeling to investigate the behavior of the p-Si/n-GaAs (RHJ) under varying temperatures and external voltages, offering insights into its performance characteristics and potential for future applications.

METHODS AND MATERIAL

We have selected a core of p-Si with a radius of 0.5 μm and a shell of n-GaAs with a radius of 1 μm within the structure as the object of this work. Based on the operating temperature of semiconductor devices made from Si and GaAs, the temperature range was selected to be between 50 K and 500 K, in steps of 50 K. The interval $d_{p-n} = r_p < r < r_n$ represents the depletion region and this depends on temperature and external voltage and is represented by the expression (1):

$$d_{p-n} = \sqrt{\frac{2(\epsilon_{GaAs} N_A + \epsilon_{Si} N_D)(\phi_{bi}(T) - U)}{q \epsilon_{Si} \epsilon_{GaAs} \epsilon_0 N_A \cdot N_D}} \quad (1)$$

where, $\epsilon_{Si}, \epsilon_{GaAs}$ are and dielectric constant of the Si and GaAs respectively, $\epsilon_0 = 8.85 \cdot 10^{-12} F \cdot m^{-1}$ electrical constant. Many articles have conducted theoretical work without considering the dependence of effective mass on temperature and electric field. To address these shortcomings, we calculated the dependence of the effective mass of electrons and holes on temperature using expression (2).

$$m_{(e,h)}^* = m(\theta) \cdot (1 + \beta_{(e,h)} \cdot (T - \theta)) \quad (2)$$

Where, $m(\theta)$ is mass, $\beta_{(e,h)}$ is the temperature coefficient of the effective mass (which can be determined experimentally or from theoretical models). θ_{GaAs} and θ_{Si} are Debye temperature GaAs and Si respectively.

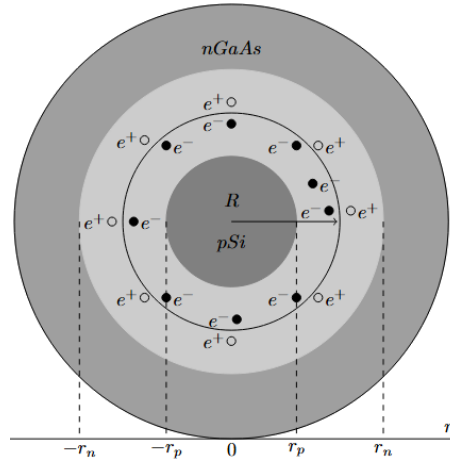


Figure 1. This figure shows a 2D cross-section of the submicron radial p-n junction structures. The light gray area represents the n-type GaAs region, the dark gray area represents the p-type Si region, and the very light gray area denotes the depletion region

Figure 1 shows the cross-sectional view of the selected p-Si/n-GaAs (RHJ) sample, cut along the Z-axis. Where r denotes the radial dimension, $\circ e^+$ and $\bullet e^-$ represents the densities of ionized N_D^+ donor and N_A^- acceptor atoms respectively, at the interface of the radial p-n heterojunction within the depletion region. If full ionization case $N_D^+ = N_D$, $N_A^- = N_A$. In Figure 1, the interval $0 < r < r_p$ represents the p-type quasi-neutral region (QNR), the interval $r_p < r < r_n$ represents the depletion region in the radial p-n heterojunction junction, the interval $r_n < r < 2R$ represents the n-type quasi-neutral region (QNR). In heterojunctions, there are differences in the conduction band ΔE_C and valence band ΔE_V at the interface, and these differences change with temperature and concentration. As a result, there is a difference in the band gap between Si and GaAs, as described by expression (3).

$$\Delta E_g(T, n, p) = \Delta E_g(T) - \Delta E_{BGN}(n, p) \quad (3)$$

Where, $\Delta E_g(T)$ is the term that depends on temperature, and $\Delta E_{BGN}(n, p)$ represents band gap narrowing, which is influenced by concentration, as described by expression (4).

$$\Delta E_{BGN}(n, p) = A \cdot \sqrt[3]{N} + B \cdot \sqrt[4]{N} + C \cdot \sqrt{N} + D \cdot \sqrt{N} \quad (4)$$

where A, B, C, and D are material-dependent semi-empirical coefficients [15]; the values for Si and GaAs are provided in Table 1. The influence of temperature and concentration on electron affinity was also examined, as expressed by equation (5).

$$\chi(T, n, p) = \chi_0 - \alpha \cdot (T - T_0) + \lambda \cdot \ln\left(\frac{(n, p)}{N_{eff}}\right) \quad (5)$$

The energy levels ΔE_C and ΔE_V are influenced by temperature. For instance, as temperature increases, the band gap can change, affecting the thermal generation of charge carriers and the performance of devices like diodes and transistors.

$$\Delta E_V(T) = \Delta E_V(0) + T \cdot (\gamma_{GaAs} - \gamma_{Si}) \quad (6a)$$

$$\Delta E_C(T) = \Delta E_V(T) + \Delta E_g(T) \quad (6b)$$

Here, γ is a coefficient that describes how the valence band shifts with temperature. $\gamma_{GaAs}, \gamma_{Si}$ are -0.006 and -0.001 eV/K respectively.

Table 1. Coefficients A, B, C, D for Si and GaAs materials

Symbol	Si		GaAs		Unit
	n-type	p-type	n-type	p-type	
A	$1.02 \cdot 10^{-8}$	$1.11 \cdot 10^{-8}$	$1.65 \cdot 10^{-8}$	$9.77 \cdot 10^{-9}$	eVcm
B	$4.15 \cdot 10^{-7}$	$4.79 \cdot 10^{-7}$	$2.38 \cdot 10^{-7}$	$3.87 \cdot 10^{-7}$	eVcm ^{3/4}
C	$1.45 \cdot 10^{-12}$	$3.23 \cdot 10^{-12}$	$1.83 \cdot 10^{-11}$	$3.41 \cdot 10^{-12}$	eVcm ^{3/2}
D	$1.48 \cdot 10^{-12}$	$1.81 \cdot 10^{-12}$	$7.25 \cdot 10^{-11}$	$4.84 \cdot 10^{-13}$	eVcm ^{3/2}

The electrostatic potential difference in the p-Si/n-GaAs (RHJ) varies with changes in the external source voltage, which can be expressed as follows (7):

$$\varphi_{bi}(T) = \Delta E_g(T) - \frac{kT}{q} \cdot \ln\left(\frac{N_A \cdot N_D}{n_{iGaAs} \cdot n_{iSi}}\right) \tag{7}$$

Here, k is the Boltzmann constant, T is the absolute temperature in Kelvin, q is the charge of an electron, N_A and N_D are acceptor and donor concentrations respectively, n_{iSi} and n_{iGaAs} are intrinsic carrier concentrations of Si and GaAs respectively. The results obtained using the formulas and material parameters outlined above are presented in the Results and Discussion section, where the findings are analyzed in relation to the initial expectations.

RESULTS AND DISCUSSION

The effective mass significantly influences the movement of electrons and holes within the crystal. It varies with temperature, affecting their behavior. Figure 2 illustrates the changes in the effective mass of electrons and holes in Si and GaAs materials.

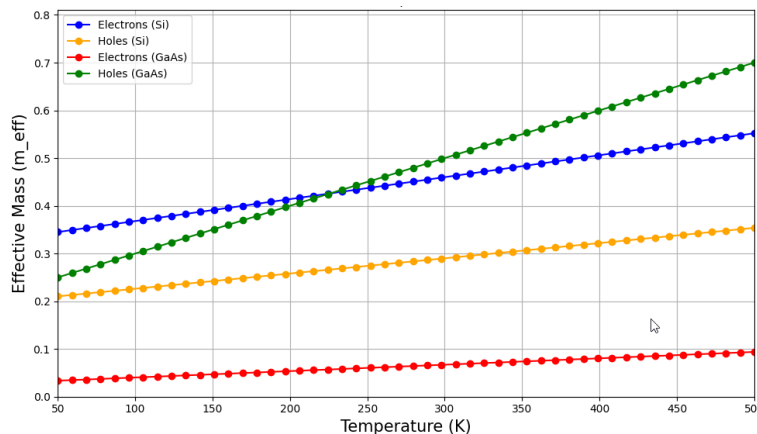


Figure 2. Effective mass of electrons and holes in Si and GaAs as a function of temperature

The plot illustrates the temperature dependence of effective masses for electrons and holes in silicon (Si) and gallium arsenide (GaAs) over a range from 50 K to 500 K. The effective mass of both carriers in each material increases slightly with temperature. In Si, electron effective mass starts at approximately 0.46m_e and hole mass at 0.29 m_e, both rising gradually. For GaAs, electrons have a lower effective mass, starting around 0.067m_e, while holes begin at 0.5m_e and exhibit a more pronounced increase with temperature.

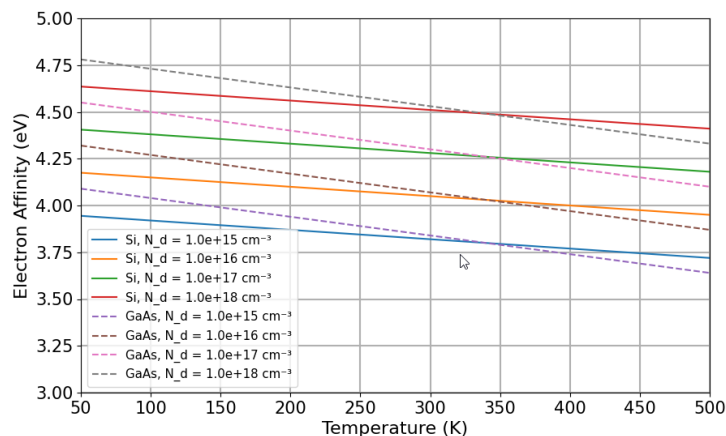


Figure 3. Electron affinity of p-Si and n-GaAs as a function of temperature.

Figure 3 illustrates that the electron affinity of both Si and GaAs decreases with varying doping concentrations over a temperature range of 50 K to 500 K. The electron affinity of GaAs is higher than that of Si up to 350 K, but beyond this temperature, the electron affinity of GaAs becomes lower than that of Si. Understanding the temperature- and doping-dependent electron affinity of Si and GaAs is essential for optimizing band alignment, carrier transport, and device stability in semiconductor applications. This knowledge enables the precise design of heterojunctions, doping profiles, and materials selection, improving the performance and reliability of devices such as transistors, solar cells, and optoelectronic components. These trends reflect material-specific characteristics, with GaAs showing a significant mass disparity between electrons and holes, benefiting high-mobility and optoelectronic applications. Understanding these variations is critical for optimizing electronic and optical device performance across a range of temperatures.

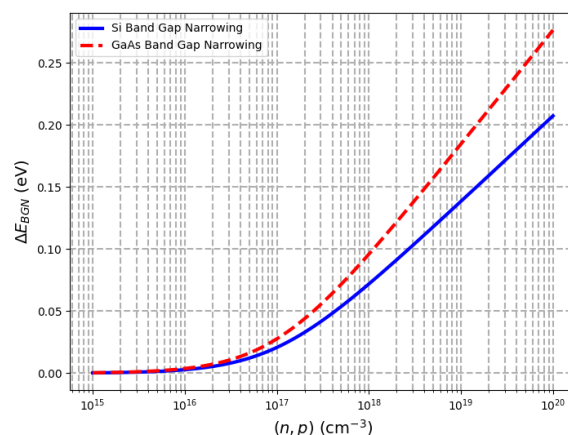


Figure 4. Band gap narrowing in Si and GaAs as a function of temperature.

Figure 4 illustrates the conduction and valence band energies as functions of temperature for Si $\Delta E_{BGN}Si(p)$ and $\Delta E_{BGN}GaAs(n)$. The blue curve represents $\Delta E_{BGN}Si(p)$, which increases from approximately 10^{15} to 10^{20} cm^{-3} as hole concentration p rises. In contrast, the red dashed line represents $\Delta E_{BGN}GaAs(n)$, which follow a similar upward trend with electron concentration n . This comparison highlights the distinct energy characteristics of Si and GaAs across a broad range of carrier concentrations, providing crucial insights into their performance in semiconductor applications.

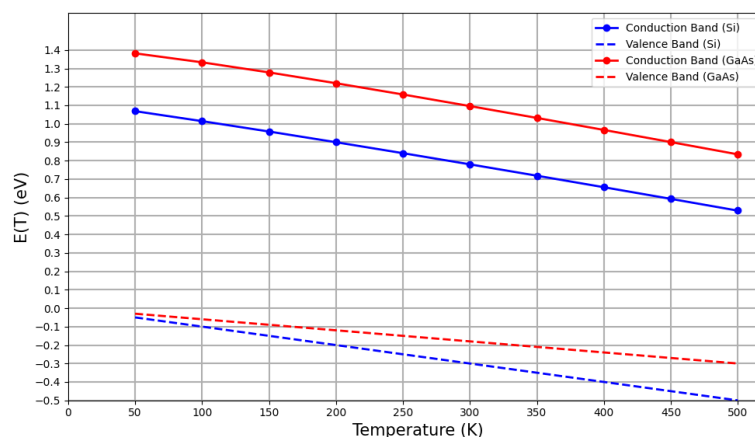


Figure 5. Conduction and valence band energies of Si and GaAs as a function of temperature.

Figure 5 illustrates the temperature dependence of conduction and valence band energies in Si and GaAs over the range of 50 K to 500 K, showing a decrease in both energy levels with increasing temperature. These changes significantly impact electronic properties, including band alignment and carrier dynamics. Understanding these variations is crucial for designing temperature-sensitive semiconductor devices, such as diodes, transistors, and heterojunctions, to ensure optimal performance across wide temperature ranges. The energies of the conduction and valence bands in Silicon and Gallium Arsenide exhibit a distinct dependence on temperature. Grasping these relationships is crucial for the effective design and optimization of semiconductor devices. Figure 6 demonstrates that the band gap and built-in potential of Si and GaAs decrease with increasing temperature, with GaAs showing a steeper decline in the band gap. These changes, influenced by material-specific properties, play a crucial role in the temperature-dependent behavior of semiconductor devices. These trends underscore the importance of temperature considerations in semiconductor device design. As both the band gap and built-in potential decrease, it becomes crucial for engineers to optimize device performance, especially in power electronics and optoelectronics, where thermal stability is vital.

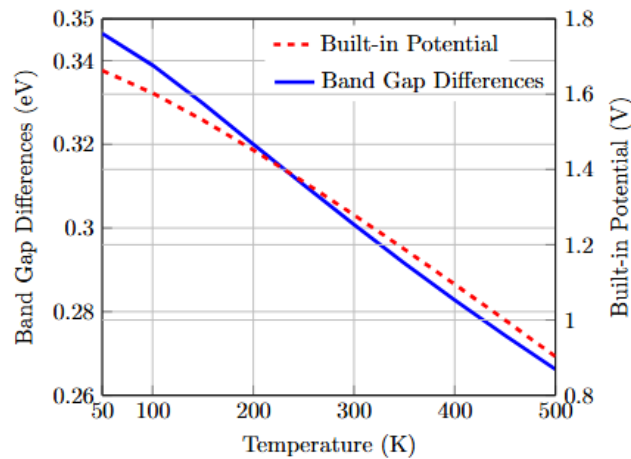


Figure 6. Differences of Band Gap and Built-in Potential as a function of Temperature

Figure 6 highlights the interplay between the band gap and built-in potential as a function of temperature, revealing their critical role in determining the electrical behavior of semiconductor devices. This understanding is vital for optimizing the performance of temperature-sensitive components like p-n junctions, LEDs, and solar cells. Our model indicates a band gap difference of 0.31 eV between GaAs and Si at 300 K, consistent with experimental data. The conduction band offset ΔE_C is calculated at 0.04 eV, while the valence band offset ΔE_V is 0.27 eV at the same temperature. The plot illustrates how temperature affects two critical semiconductor parameters: Band Gap Differences and Built-in Potential. As temperature rises from 50 K to 500 K, both the band gap and built-in potential decrease: Band Gap Differences, the band gap narrows from approximately 0.35 eV to 0.26 eV due to increased lattice vibrations and thermal excitation, which reduce the energy needed for electron transitions. A narrower band gap can increase intrinsic carrier concentrations, enhancing conductivity but also potentially causing unwanted leakage currents in high-temperature devices. Built-in Potential, the built-in potential decreases from about 1.66 V to 0.9 V, indicating a weakening of the internal electric field. This change suggests that thermal effects significantly influence charge carrier dynamics, potentially reducing the efficiency of devices reliant on strong potential barriers, such as diodes and transistors, in high-temperature applications.

This analysis highlights the need for further research into the mechanisms behind these temperature effects and their implications for specific device architectures. Figure 7 shows how the band gap for silicon (Si) and gallium arsenide (GaAs) changes with temperature from 40 K to 500 K. GaAs start with a higher band gap of 1.52 eV at 40 K, decreasing to about 1.35 eV at 500 K, indicating greater thermal sensitivity than Si. This temperature dependence in GaAs can affect its performance at high temperatures but still makes it ideal for optoelectronic applications due to its direct band gap, which benefits devices like LEDs and laser diodes. Overall, understanding these thermal properties helps in designing reliable devices optimized for Si's stability or GaAs's high-frequency and optical capabilities.

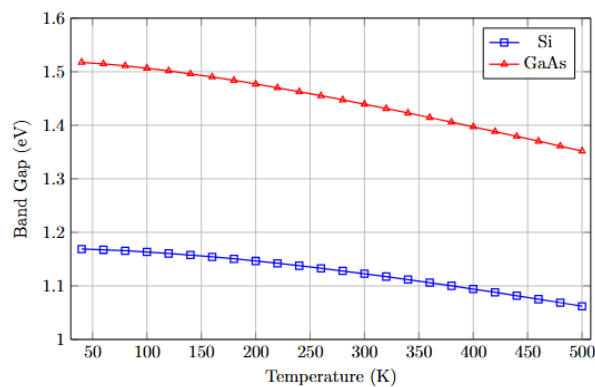


Figure 7. Band gaps of Si and GaAs as a function of temperature

Figure 8 shows that the intrinsic carrier concentration, for Si and GaAs rises exponentially from 50 K to 500 K due to thermal generation of carriers. GaAs, with its narrower band gap, reaches higher $n_i(T)$ values, indicating greater thermal sensitivity compared to Si. Here, majority carrier concentration $p_p = n_n = N_A = N_D = 2 \cdot 10^{16} \text{ cm}^{-3}$, minority carrier concentration $p_n = n_i^2 / N_D$ and $n_p = n_i^2 / N_A$. Here, $n_i = 1.7 \cdot 10^6 \text{ cm}^{-3}$ is the intrinsic concentration, for GaAs, $n_i = 1.5 \cdot 10^{10} \text{ cm}^{-3}$ for Si at 300 K. This temperature-dependent behavior impacts conductivity, with higher temperatures

potentially affecting device stability. Si's stability is ideal for general electronics, while GaAs's thermal sensitivity and direct band gap make it well-suited for optoelectronic and high-frequency applications, especially in controlled settings. These insights are essential for optimizing device design across different thermal conditions.

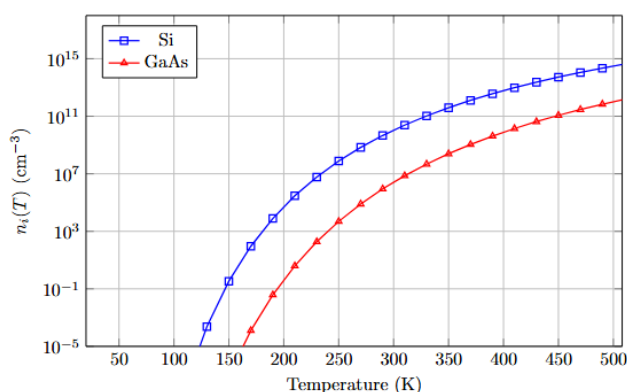


Figure 8. Intrinsic carrier concentration of Si and GaAs as a function of temperature.

CONCLUSIONS

In conclusion, our analytical study of the p-Si/n-GaAs radial heterojunction, specifically with a core radius of 0.5 μm and a shell radius of 1 μm , provides significant insights into its electrophysical features over a temperature range of 50 K to 500 K. We observed that the thickness of the depletion region increases with rising temperature, reflecting the complex dynamics within the heterojunction. At 300 K, the band gap difference between GaAs and Si was determined to be 0.31 eV, which aligns closely with experimental data, while the conduction band offset was calculated at $\Delta E_C = 0.04$ eV and the valence band offset at $\Delta E_V = 0.27$ eV. Additionally, our analysis showed that band gap narrowing (BGN) decreases by 2 meV as doping concentrations increase from $2 \cdot 10^{15}$ to $2 \cdot 10^{18}$. Moreover, we found that the built-in potential of the p-Si/n-GaAs heterojunction decreases by 76 mV with an increase in temperature. These quantitative findings highlight the importance of considering both the geometric parameters and doping concentration in the design and optimization of radial heterojunctions, providing a solid foundation for future advancements in semiconductor device applications.

ORCID

© Jo'shqin Sh. Abdullayev, <https://orcid.org/0000-0001-6110-6616>

© Ibrokhim B. Sapaev, <https://orcid.org/0000-0003-2365-1554>

REFERENCES

- [1] R. Elbersen, R.M. Tiggelaar, A. Milbrat, G. Mul, H. Gardeniers, and J. Huskens, *Advanced Energy Materials*, **5**(6), 1401745 (2014). <https://doi.org/10.1002/aenm.201401745>.
- [2] E. Gnani, A. Gnudi, S. Reggiani, and G. Baccarani, *IEEE Trans. Electron Devices*, **58**(9), 2903 (2011). <https://doi.org/10.1109/TED.2011.2159608>.
- [3] Abdullayev, J. Sh., & Sapaev, I. B. (2024). Optimization of The Influence of Temperature on The Electrical Distribution of Structures with Radial p-n Junction Structures. *East European Journal of Physics*, (3), 344-349. <https://doi.org/10.26565/2312-4334-2024-3-39>
- [4] Abdullayev, J. Sh., Sapaev, I. B. (2024). Оптимизация влияния легирования и температуры на электрофизические характеристики p-n и p-i-n переходных структур. *Eurasian Physical Technical Journal*, 21(3(49)), 21–28. (<https://doi.org/10.31489/2024No3/21-28>).
- [5] O.V. Pylypova, A.A. Evtukh, P.V. Parfenyuk, I.I. Ivanov, I.M. Korobchuk, O.O. Havryliuk, and O.Yu. Semchuk, *Opto-Electronics Review*, **27**(2), 143 (2019). <https://doi.org/10.1016/j.opelre.2019.05.003>.
- [6] R. Ragi, R.V.T. da Nobrega, U.R. Duarte, and M.A. Romero, *IEEE Trans. Nanotechnol.* **15**(4), 627 (2016). <https://doi.org/10.1109/TNANO.2016.2567323>.
- [7] Abdullayev, J., & Sapaev, I. B. (2024). Factors Influencing the Ideality Factor of Semiconductor p-n and p-i-n Junction Structures at Cryogenic Temperatures. *East European Journal of Physics*, (4), 329-333. <https://doi.org/10.26565/2312-4334-2024-4-37>
- [8] R.D. Trevisoli, R.T. Doria, M. de Souza, S. Das, I. Ferain, and M.A. Pavanello, *IEEE Trans. Electron Devices*, **59**(12), 3510 (2012). <https://doi.org/10.1109/TED.2012.2219055>.
- [9] N.D. Akhavan, I. Ferain, P. Razavi, R. Yu, and J.-P. Colinge, *Appl. Phys. Lett.* **98**(10), 103510 (2011). <https://doi.org/10.1063/1.3559625>.
- [10] A. V. Babichev, H. Zhang, P. Lavenus, F.H. Julien, A. Y. Egorov, Y.T. Lin, and M. Tchernycheva, *Applied Physics Letters*, **103**(20), 201103 (2013). <https://doi.org/10.1063/1.4829756>.
- [11] D.H.K. Murthy, T. Xu, W.H. Chen, A.J. Houtepen, T.J. Savenije, L.D.A. Siebbeles, *et al.*, *Nanotechnology*, **22**(31), 315710 (2011). <https://doi.org/10.1088/0957-4484/22/31/315710>.
- [12] B. Pal, K.J. Sarkar, and P. Banerji, *Solar Energy Materials and Solar Cells*, **204**, 110217 (2020). <https://doi.org/10.1016/j.solmat.2019.110217>.
- [13] Abdullayev, J. and Sapaev, I. 2024. Modeling and calibration of electrical features of p-n junctions based on Si and GaAs. *Physical Sciences and Technology*. 11, 3-4 (Dec. 2024), 39–48. <https://doi.org/10.26577/phst2024v11i2b05>.

- [14] I. Aberg, G. Vescovi, D. Asoli, U. Naseem, J.P. Gilboy, C. Sundvall, and L. Samuelson, IEEE Journal of Photovoltaics, **6**(1), 185 (2016). <https://doi.org/10.1109/JPHOTOV.2015.2484967>.
- [15] S. C. Jain and D. J. Roulston, "A Simple Expression for Band Gap Narrowing (BGN) in Heavily Doped Si, Ge, GaAs and $\text{Ge}_x\text{Si}_{1-x}$ Strained Layers," Solid-State Electronics, vol.34, no. 5, pp. 453–465, 1991.

АНАЛІТИЧНИЙ АНАЛІЗ ОСОБЛИВОСТЕЙ РАДІАЛЬНИХ ГЕТЕРОПЕРЕХОДІВ GaAs/Si: ВПЛИВ ТЕМПЕРАТУРИ ТА КОНЦЕНТРАЦІЇ

Джошкін Ш. Абдуллаєв^a, Іброхім Б. Сапаєв^{a,b}

^aНаціональний дослідницький університет ТПАМЕ, фізико-хімічний факультет, Ташкент, Узбекистан

^bЗахідно-Каспійський університет, Баку, Азербайджан

У цій статті ми аналітично досліджуємо електрофізичні особливості радіального гетеропереходу p-Si/n-GaAs у діапазоні температур від 50 К до 500 К з кроком 50 К, враховуючи різні концентрації легування. Аналіз охоплює звуження енергетичної щільності, різницю в енергетичній щільності між GaAs і Si як функцію температури, а також вбудований потенціал залежно від температури. Зокрема, ми зосереджуємо увагу на ядрі з p-Si з радіусом 0,5 мкм та оболонці з n-GaAs з радіусом 1 мкм у структурі. Наші результати показують, що товщина області збіднення в p-Si/n-GaAs збільшується зі зростанням температури. Різниця енергетичної щільності між GaAs і Si становить 0,31 еВ при 300 К у нашій моделі, що добре узгоджується з експериментальними результатами. Крім того, зсув зони провідності $\Delta E_c=0,04$ еВ та зсув валентної зони $\Delta E_v=0,27$ еВ були обчислені при 300 К. При зміні концентрації легування від $2 \cdot 10^{15}$ до $2 \cdot 10^{18}$ звуження енергетичної щільності зменшується на 2 мєВ. Додатково, вбудований потенціал p-Si/n-GaAs зменшується на 76 мВ зі збільшенням температури.

Ключові слова: радіальний p-n перехід; світлова пастка; зовнішні фактори; вольт-фарад; гетероструктури; радіальний гетероперехід; звуження енергетичної щільності; кріогенні температури